HHS Public Access

Author manuscript

Dev Biol. Author manuscript; available in PMC 2024 July 01.

Published in final edited form as:

Dev Biol. 2023 July ; 499: 10–21. doi:10.1016/j.ydbio.2023.04.001.

Aberrant Differentiation of Second Heart Field Mesoderm Prefigures Cellular Defects in the Outflow Tract in Response to Loss of FGF8

Sophie Astrof[1], **Cecilia Arriagada**[1], **Yukio Saijoh**[2], **Alexandre Francou**[3], **Robert G. Kelly**[3], **Anne Moon**[4,5,6]

[1.]Department of Cell Biology and Molecular Medicine, New Jersey Medical School, Rutgers Biomedical and Health Sciences, Newark, NJ, USA

[2.]Department of Neurobiology and Anatomy, University of Utah, Salt Lake City, UT, USA

[3.]Aix-Marseille Université, CNRS UMR 7288, Developmental Biology Institute of Marseille, Marseille, France

[4.]Department of Molecular and Functional Genomics, Weis Center for Research, Geisinger Clinic, Danville, PA, USA

[5.]Department of Human Genetics, University of Utah, Salt Lake City, UT, USA

[6.]The Mindich Child Health and Development Institute, Hess Center for Science and Medicine at Mount Sinai, New York, NY, USA

Abstract

Development of the outflow tract of the heart requires specification, proliferation and deployment of a progenitor cell population from the second heart field to generate the myocardium at the arterial pole of the heart. Disruption of these processes leads to lethal defects in rotation and septation of the outflow tract. We previously showed that Fibroblast Growth Factor 8 (FGF8) directs a signaling cascade in the second heart field that regulates critical aspects of OFT morphogenesis. Here we show that in addition to the survival and proliferation cues previously described, FGF8 provides instructive and patterning information to OFT myocardial cells and their progenitors that prevents their aberrant differentiation along a working myocardial program.

INTRODUCTION

Mesodermal cells destined to contribute to the heart arise in the anterior portion of the primitive streak in the early mouse embryo. At approximately embryonic day (E) 7.5, these cells migrate to the anterior ventral aspect of the embryo and form a bilaterally symmetric domain called the cardiac crescent (Lough and Sugi, 2000; Schultheiss et al., 1995; Yutzey and Kirby, 2002). It has long been established that cells that contribute to different portions of myocardium accrue to the heart at different times (de la Cruz et al., 2001; de la Cruz et al., 1977). Lineage analyses in the chick demonstrated that myocardial cells destined for

Corresponding Author: Anne Moon ammoongrs@outlook.com.

the right ventricle (RV), conus (proximal OFT) and the truncus (distal OFT) are deployed at different times (Mjaatvedt et al., 2001; Waldo et al., 2001). Retrospective clonal analyses in mouse discerned two myocardial lineages in the embryonic heart: the first lineage contributed to all segments except the OFT, and the second, to all segments but the left ventricle (Meilhac et al., 2004). Thus, mesoderm in the cardiac crescent is considered as two "fields" of heart precursors distinguished by their relative location in the crescent, the time at which they accrue to the heart proper, and the location of their derivatives within the heart (Buckingham et al., 2005). After formation of the primary heart tube from cells in the first heart field, myocardium begins to accrue to both arterial and venous poles from progenitors in the second heart field (SHF). Looping of the heart tube creates the outer and inner curvatures of the heart. Cells in the outer curvature contribute to the working or chamber myocardium and are in a more differentiated state than those of the developing OFT on the inner curvature which retain molecular, proliferative and electrophysiologic properties of primary, non-working myocardium (Christoffels et al., 2000; Kelly et al., 2001; Mjaatvedt et al., 2001; Waldo et al., 2001; Zaffran et al., 2004). As such, OFT myocardial cells have specialized secretory and signaling functions that coordinate its nonworking myocardial development with interacting endothelial and neural crest cell populations that are critical for proper OFT morphogenesis.

We previously reported that loss of FGF8 signaling in the SHF in *Fgf8 fl/−; Isl1Cre* conditional mutants causes a severe OFT defect called Persistent Truncus Arteriosus (PTA) in 100% of conditional mutants (Park et al., 2006). We subsequently found that this was due to disruption of an FGF autocrine signaling loop in SHF mesoderm which resulted in decreased survival and proliferation of these OFT myocardial progenitors (Park et al., 2008).

Here we investigate the cellular and molecular defects in the outflow tract myocardium of these mutants and in their progenitors in the SHF. We found that in addition to the survival and proliferation defects in the SHF we previously described, loss of FGF8 results in abnormal SHF and OFT epithelia with disrupted apical-basal and planar polarity. Further, we show that in the absence of the instructive information provided by FGF8, the OFT myocardium abnormally differentiates to express a working myocardial transcriptional program that is prefigured in the abnormal expression of a myocardial program in the SHF itself.

RESULTS

Myocardium in the outflow tract of *Fgf8;Isl1Cre* mutants is disorganized and has abnormal polarity.

To further define the cellular and molecular defects of *Fgf8* mutants that ultimately result in PTA, we examined the cellular organization of the OFT myocardium. As progenitor cells migrate from the SHF and differentiate, they are incorporated and organized into a contracting, functional myocardial epithelium with planar and apical-basal polarities and a nonworking myocardial program. Longitudinal H&E sections through the OFT of verapamil-relaxed, control ($Fgf8^{fl/+,}$ no cre) E10.5 mouse hearts reveal the normal organized epithelium of the OFT myocardium with tightly interdigitated and planar-aligned cells (Figure 1A, black arrowheads). In E10.5 *Fgf8* conditional mutants ($Fgf8^{fl/-}$*; Isl1Cre*) the

OFT myocardial epithelium is disorganized (Fig. 1B, black arrows), the amount of the cardiac jelly is decreased (black double-headed arrows in A and B are the same size), and fewer mesenchymal cells derived from endocardial EMT (mes) are present. Dark field, high magnification images show that control myocardial cells are aligned along the longitudinal axis in the plane of the section; the cells and nuclei are elongated (Fig. 1 C, E). In contrast, the mutant myocardial cells are rounded and project in all directions with no apparent plane of alignment; there are frequent cell clusters protruding out of the plane of the OFT wall (white arrows, Fig. 1 D, F). Immunohistochemical staining for β-catenin and filamentous actin highlights these findings and shows abnormally localized and apparently increased β-catenin in the mutants (compare Fig. 1G to 1I). Actin fibers are clear and aligned perpendicular to the longitudinal plane of the OFT in controls (Fig. 1H) while in mutants, the fibers are poorly organized and staining is present at the cell periphery (Fig. 1J, arrowheads and arrows, respectively).

Specific adhesive properties and intercellular connections are required for the OFT myocardial epithelium to function as a secretory and electrical syncytium. Correct apical-basal polarity must be established for directional secretion of cardiac jelly to generate the endocardial cushions and of signaling molecules that regulate endothelial and neural crest migration. We used immunohistochemistry to evaluate basement membrane characteristics and polarity of the transition zone (the distal OFT and adjacent SHF) in E9.5 control and *Fgf8;Isl1Cre* mutant embryos. Fibronectin is expressed in the SHF and signals via Integrin α5 to drive normal OFT and pharyngeal arch artery development (Mittal et al., 2010, 2013). As shown in the sagittal views of the transition zone from the SHF to the OFT in Figure 2, Fibronectin and Integrin α5 are normally co-assembled in the basement membrane at the basal surface of the epithelium (Fig. 2A-E'). In the absence of FGF8 there is less visible fibronectin and it is irregularly distributed (Fig. 2 G, H, J'). Integrin α5 is restricted to the basal surface of the epithelium in association with fibronectin in controls (arrowheads in Fig. 2E') while in the mutants Integrin α5 staining is redistributed and abnormally present around lateral and apical surfaces (arrows, Fig. 2J'). Integrin β1 is normally enriched at the basal surface while β-catenin is present in punctate apicolateral signals in the adherens junctions (Fig. 2K-N', arrowheads in M' for Integrin β1, N' for β-catenin) however, in mutants, Integrin β1 and β-catenin surround the cells (arrows, Fig. 2 Q' for Integrin β1, R' for β-catenin) and the level of β-catenin appears increased, most notably at the apical surface (Fig. 2 R' arrows, note that in the mutants, the relative levels of β-catenin in the SHF/OFT and the adjacent endoderm are similar, while in controls, β-catenin levels are relatively higher in the endoderm compared to the OFT/SHF. Increased levels of β-catenin are also apparent in panel I of Figure 1). Podocalyxin is a transmembrane glycoprotein involved in the regulation of both adhesion and cell morphology; it was first described as an apical cytoskeletal marker in MDCK cells as gp135 (Meder et al., 2005; Ojakian and Schwimmer, 1988). Here we found it is strictly restricted to the apical surface in the OFT and SHF of controls (Fig. 2S-V', arrowheads in V') but its signal is irregular and appears to surround the aberrantly positioned, clumped cells in mutants (Fig. 2 W-Z', arrows in Z').

Further evidence of altered polarity is the abnormal pattern of Scribble and atypical Protein Kinase C zeta (aPKCζ) shown in Supplemental (S.) Figure 1. This figure shows

transverse sections that progress from the rostral region of the pharynx/OFT/SHF (panels A, B) caudally to the posterior SHF adjacent to the sinus venosus (from C-G, and D-H). Images I-P show digital zoom views of the white-boxed, correspondently labeled regions in the top panels. In the rostral region of the mutants, there is a paucity of cells in the SHF and their organization and the pattern/quantity of both markers along the surface of the SHF and distal OFT appears abnormal (S. Fig. 1: compare arrowheads in I and M [control] to arrows in K and O [mutant]). In contrast, staining and cell morphology are comparable in mutants and controls in the caudal/posterior SHF (Suppl. Fig. 1: J versus L and N versus P) while abnormalities in the endoderm persist in this region of the pharynx (labeled “e” lining the foregut in Suppl. Fig. 1, panels I-P). Altogether, these microscopic and immunohistochemical data show altered epithelial features, including abnormal cell polarity and ECM accumulation, in the SHF and within the distal OFT of conditional mutant embryos.

Transcriptional profiling reveals abnormal differentiation of outflow tract myocardial cells to a working myocardial program in *Fgf8* mutants.

To obtain insight into underlying transcriptional events that could contribute to the aberrant OFT cell morphology and polarity, we mined our previously reported and validated transcriptional profiles of the OFTs of E9.5 *Fgf8; Isl1Cre* mutants and controls (Park et al., 2008). Heatmaps of curated markers show widespread dysregulation of adhesion and migration genes (S. Fig. 2A: desmosomal and other cadherins, integrins, guidance molecules) as well as genes in the canonical Wnt and planar cell polarity pathways (S. Fig. 2B). GREAT analysis of the OFT transcriptional profiles showed that the most enriched biologic process term in genes downregulated by 1.5-fold or more in the mutants (S. Fig. 3A) was “desmosome organization” consistent with the heat map in S. Figure 2A. while most other terms were related to EMT and outflow tract morphogenesis, as expected. The enriched term “negative regulation of muscle cell differentiation” in the downregulated gene set is notable given that in the upregulated gene set, the most enriched biologic process was “muscle cell development” (S. Fig. 3B).

These findings led us to question if the cellular abnormalities in the OFT of *Fgf8* mutants could be the result of abnormal differentiation. Since regions of the developing heart have distinct transcriptional signatures, we performed microdissection to separate the distal and proximal segments of the OFT from one another and from the right and left ventricles (Fig. 3A). We then used RT-PCR to examine the expression of genes that reflect these different segments of the heart (Fig. 3, groups C-F). The schematics to the left of each group of PCR results show the pattern of expression levels for that group of genes in the different segments - while somewhat arbitrary, these patterns/groups fit with *in situ* findings by us and others as documented in MGI. Group C genes are primary/nonworking OFT markers with much higher expression in the distal OFT than other segments while in group D, the expression in the proximal OFT is closer to that seen in the distal OFT. Groups E and F show relative expression levels of known working/chamber epicardial and myocardial markers, some of which are also detected in the proximal OFT as dissected in this experiment (Group E). These experiments confirm/establish distinct gene expression patterns in microdissected regions and show that we can isolate different parts of the forming heart.

We then interrogated the OFT genome-wide transcriptional data comparing controls and mutants for expression of these and other markers of primary and working myocardium, as shown in the heat map in Figure 3G. This revealed that the *Fgf8* mutant OFT myocardium fails to attain a nonworking myocardial identity: there is decreased expression of known OFT primary/nonworking markers while working myocardial/chamber genes are over-expressed (Fig. 3G), as also detected by the GREAT tool (Suppl. Fig. 3A, B). For example, BMP10 is a proliferative factor required for chamber expansion and trabecular development and is normally expressed only transiently in developing trabecular myocardium (Shou et al., 1998); it is aberrantly expressed in the mutant OFT here. *Nppa* is a well-established chamber marker that is increased in the mutant OFT, as are *Irx1, 2, 5* and *6*. In contrast, *Irx4* is the only *Irx* gene normally expressed in the OFT (Kim et al., 2012) and it is downregulated here. *Chac1* is a marker of left ventricular myocardium (Frank et al., 2012) and is also upregulated in mutant OFT, as is *Sema3e,* which is widely expressed in different working myocardial populations (Sandireddy et al., 2019). Moreover, numerous myosin heavy and light chains are aberrantly expressed in the mutant OFT as are cardiac troponins (*Tnnt2, Tnnt3*), myogenic factors, and myosin and titin binding proteins. As far as downregulated OFT markers, in addition to the OFT specific transcripts shown in groups C and D, OFT/progenitor genes such *Nkx2.6* (Biben et al., 1998), *Hand2*, *Msx1* and *Msx2* (Chen et al., 2007) are downregulated as are members and targets of the Tgfβ, BMP, Wnt and Notch pathways (in addition to those included in this heatmap, other downregulated members and targets of these pathways are described in detail in Park et. al. 2008 (Park et al., 2008) and in S. Figure 2. Upregulation of multiple working myocardial transcripts in the OFT and downregulation of myocardial progenitor and OFT markers are consistent with abnormal differentiation of the mutant OFT to a working myocardial program.

Subpopulations of OFT progenitors fail to populate the outflow tract in *Fgf8* mutants.

Outflow tract progenitors in the SHF are parcellated into subdomains with distinct molecular programs and fates as evidenced by "cardiosensor" transgenic reporter lines (Theveniau-Ruissy et al., 2008). Disruption of these programs, and/or abnormal deployment of cells from these subdomains could contribute to the OFT defects seen in *Fgf8* mutants. A region of SHF mesoderm and myocardium in the left, inferior wall of the e9.5-10.5 OFT is labeled by the *y96-Myf5-nlacZ-16* transgene (96-16, Fig. 4 A-D); rotation of the conotruncus brings this segment of myocardium to the anterior/ventral region surrounding the pulmonary valve by E12.5 (S. Fig. 4A) (Bajolle et al., 2006). In contrast, the *A17-Myf5-nlacZ-T55* transgene (T55) labels a population in the superior wall of the early OFT (Fig. 4 N-Q) and at the base of the aorta in the septated OFT (S. Fig. 5D) (Bajolle et al., 2008). We assayed the fate of these populations in *Fgf8* mutants and controls in whole mount and microdissected Lacz stained embryos at E9.5 (Fig. 4) and E12.5 (S. Fig. 4). In *Fgf8* mutants there is markedly decreased activity of the 96-16 reporter in the pharyngeal arches/SHF and in the OFT itself (Fig. 4F-I). While not as severe as in conditional *Fgf8* mutants, there was decreased activity of the 96-16 reporter in the SHF in *Isl1Cre/+* embryos although the location of the reporter cells that are present in the OFT is normal (Fig. 4M, S. Fig. 4C). The 96-16 transgene integration site has been mapped to a genomic region near *Semaphorin3c* and the transgene is expressed in the pattern of *Sema3c.* We assayed *Sema3c* transcripts in E9.5 *Isl1Cre*/+ embryos and found that unlike the reporter, expression of the gene was only

modestly decreased in the SHF and OFT (S. Fig. 5). Activity of the T55 reporter was also markedly decreased in the OFT and SHF of *Fgf8* mutants (Fig. 4R-U) but unaffected in Isl1Cre heterozygotes (Fig. 4 V-Y, S. Fig. 4F). This transgene has been mapped to a site near *Hes1* and recapitulates its expression in several domains (Rochais et al., 2009). Overall, the loss of signal of these cardiosensor lines far exceeds the extent of apoptosis we detected in the SHF in these mutants (Park et al., 2006) thus, these data show that the specification and/or expansion of two different SHF subdomains is disrupted in *Fgf8* mutants and that the 96-16-labeled progenitor population is also sensitive to haploinsufficiency for Isl1.

Defects in the *Fgf8* mutant outflow tract myocardium are prefigured by premature myocardial differentiation of second heart field mesoderm.

We next sought to examine the transcriptional signature of the SHF mesoderm to understand the effects of loss of the FGF8 autocrine signaling loop on a transcriptome-wide scale and how abnormalities in the SHF could contribute to the aberrant differentiation of the SHF progeny in the OFT. We developed a method for separating the SHF mesoderm from the adjacent ectoderm, endoderm and heart based on gentle tissue dissociation with pancreatin/trypsin and microdissection. As shown in Figure 5A-C, this technique allows stepwise isolation of each germ layer from early mouse embryos. For our experiment, we performed the microdissection on E9.5 embryos (23-27ss, Fig. 5D) when mesoderm from the SHF is being deployed into the OFT. To test the precision of our dissection we used the *Wnt1Cre*, *Mesp1Cre*, and the *Rosa*^{mTmG} reporter lines to label neural crest and mesoderm in our dissections, respectively. Based on the *Wnt1Cre* driver, we detect a small amount of neural crest present in the ectodermal and endodermal dissected components (Fig. 5E, GFP signal). Relevant here is the neural crest, labeled with GFP, from pharyngeal arch 2 present in the mesodermal dissection (Fig. 5E, neural crest and SHF mesoderm). Further dissection of one half of this tissue to remove some of the neural crest is shown in Figure 5F using the *Mesp1Cre* driver to label mesoderm with GFP. Relatively less neural crest is present, but the residuum would still be anticipated to contribute to the transcriptional profiles we obtain from these samples.

We then performed microarray analysis of transcripts in the microdissected SHF mesoderm (and accompanying neural crest) in *Fgf8* mutants and controls (Table 1). As expected, downstream transcriptional targets of FGF8 such as *Etv4* and *Etv5* were decreased as were transcripts for other FGF ligands (*Fgf3, 4* and *15*) while *Fgf10* expression was unaffected (as we previously reported (Park et al., 2008)); of these, FGF3 and FGF15 have known roles in OFT morphogenesis (Urness et al., 2011; Vincentz et al., 2005). GREAT analysis did not detect any enriched Biologic Processes among downregulated genes (the DAVID tool revealed only 2 functional annotation clusters that were enriched greater than 2-fold; these clusters contain the expected terms organ morphogenesis and FGF signaling, not shown). GREAT analysis of the upregulated gene set was very informative as it showed the most enriched biologic processes were related to cardiac muscle, muscle contraction and sarcomeric structure and organization (S. Fig. 6A). As expected, there were enriched biologic processes likely attributable to the neural crest component (sensory perception of smell, olfactory transduction, not shown). We examined the genes in the cardiac-enriched processes and also mined the data for functionally related transcripts,

known SHF markers, and other transcripts that were dysregulated in the OFT analysis for comparison (Fig. 6A). The majority of SHF markers that were significantly changed were downregulated, while genes encoding chamber and muscle proteins are upregulated. We used immunofluorescence to determine if these transcriptional changes were associated with aberrant protein expression in the SHF and transition zone and found abnormal staining for Titin and MF-20 in the SHF and transition zone (Fig. 6 B-G). This aberrant staining was observed in 50% of mutants examined (n=6). Also consistent with an abnormal working myocardial phenotype is the observation that the cellular organization and both the apparent intensity and pattern of β-catenin staining in the TZ/SHF of mutants was comparable to that of right ventricular freewall working myocardium (S. Figure 7).

DISCUSSION

Our data provide new evidence that FGF signaling has instructive roles in the SHF and its progeny in the OFT myocardium in addition to the proliferative and survival roles previously described (Park et al., 2006; Park et al., 2008). We show that these signals are required to prevent aberrant differentiation of the OFT myocardium along a working myocardial program and to prevent premature differentiation of SHF cells into cardiomyocytes.

An asymmetrical distribution of junctional complexes (adherens and tight junctions) and other proteins is required for establishing and maintaining cell polarity in epithelial cells; apical-basal and planar polarity are not only required for efficient contractile and electrical coupling of the nascent OFT myocardium but also for directed secretion of ECM and signaling molecules and for oriented cell growth. Our data indicate that the organization and shape of *Fgf8; Isl1Cre* mutant OFT myocardial cells are abnormal and that the transcriptional profile of determinants of apical-basal and planar cell polarity and cell adhesion is disrupted in these cells. We found cellular evidence of altered cell polarity and epithelial organization in the OFT and the SHF evident in mislocalization of basolateral and apical proteins including Integrin β1, Fibronectin, Integrin α5, β-catenin, Podocalyxin, Scribble and Atypical Protein Kinase C zeta. These changes were accompanied by abnormal transcript levels in the OFT for major adhesion and migration genes as well as genes in the canonical Wnt and PCP pathways. We previously reported the abnormalities in BMP and Tgfβ pathway transcripts relevant to EMT in the outflow tract that were detected in this experiment (Park et al., 2008).

The importance of the noncanonical/PCP pathway for convergent extension/planar organization as seen in the neural tube and cochlea has been extended to OFT morphogenesis (Hamblet et al., 2002; Kibar et al., 2001; Kioussi et al., 2002; Li et al., 2019; Montcouquiol et al., 2003; Sinha et al., 2012). Decreased expression of the noncanonical Wnt ligand Wnt11 and Tgfβ pathway members, as seen in *Fgf8* mutant OFTs [S. Fig. 2B, (Park et al., 2008)], likely play a role in the phenotype as *Wnt11* null mutants have OFT defects (DORV, TGA) associated with decreased expression of Tgfβ2 (Zhou et al., 2007). Similarly, Tgfβ2 null mutants have DORV and decreased cushion jelly (Bartram et al., 2001).

Canonical Wnt signaling is required for normal deployment and differentiation of SHF progenitors to support OFT and RV formation and remodeling (Ai et al., 2007; Cohen et al., 2007; Lin et al., 2007). Indicators of disrupted Wnt signaling in the OFT include altered transcript levels for Wnt potentiators and effectors (*Lgr4, Lgr5, Trib2, Trib3, Tcf7, Rspo3*), antagonists (*Wisp1* and *Dkk1*), and receptors and coreceptors (*Lrp5, Fzd7*). Expression of *Cthrc1* is decreased and this factor activates both the Wnt and PCP pathways by stabilizing the interaction between Wnt ligands and their Frizzled or Receptor Tyrosine Kinase Like Orphan Receptor 2 (ROR2) receptors (Yamamoto et al., 2008). Balancing between canonical and noncanonical Wnt signaling plays a role in promotion or prevention of differentiation in the SHF (Ruiz-Villalba et al., 2016).

Studies in *Scrib* mutant mice have confirmed the importance of cell polarity for myocyte organization, adhesion, migration, and secretory function and an important role for this factor during OFT and chamber morphogenesis. *Scrib* mutant cardiomyocytes are abnormally shaped and disorganized in association with altered localization of N-cadherin as well as β-catenin (Phillips et al., 2007), as we see here in the mutant OFT in association with abnormal localization of Scribble in the OFT and SHF

Aside from increased expression of working myocardial markers/chamber genes and sarcomeric proteins in both the mutant OFT and SHF, increased expression of *WT1* and *Tbx18*, (both in the mutant OFT and SHF) as well as *Fgf9* (in mutant OFT) is intriguing because these are markers of epicardium and epicardial-derived myocardium and may be indicative of at least a subset of cells adopting an alternate SHF-derived identity (Cai et al., 2008; Zhou et al., 2008).

Downregulation of *Nkx2.6* in both OFT and SHF is also notable in that although rarely discussed in the literature on the embryologic origins of OFT defects, mutations in *NKX2.6* in humans are associated with PTA and other OFT defects (Heathcote et al., 2005). In the mouse, this gene is expressed as early as E8.0 in the pharyngeal mesoderm and at both the venous and arterial poles of the early heart tube, with subsequent high-level expression at E9.5 in the SHF and OFT (Biben et al., 1998; Liao et al., 2008). Furthermore, *Nkx2.6* is regulated by Tbx1 in the SHF (Liao et al., 2008) and we have previously demonstrated that loss of Tbx1 downregulates expression of FGF receptor 1 in the SHF (Park et al., 2006). Here, we also note overlap between the upregulated gene profile detected in the caudal pharynx of *Tbx1* null mutants (Liao et al., 2008) and the panel of upregulated genes in the SHF shown in Figure 6. This finding reinforces the concept that Tbx1 and FGF8 regulate common pro-proliferation/anti-differentiation programs in the pharynx and SHF required for OFT development (Boyett et al., 2006; Frank et al., 2002; Guo et al., 2011).

Molecular and fate mapping data indicate that specific regulatory programs determine the identity and fate of subregions of the SHF containing arterial pole progenitors (Buckingham et al., 2005). For example, the expression of *Fgf10* in different SHF subdomains is regulated by distinct enhancers (Watanabe et al., 2012). T The precursors in different subdomains are located in different regions within the SHF (Bajolle et al., 2008) and so they are exposed to, and likely require, different signals to acquire their identity and achieve their fate in the OFT. The observation that both the 96-16 and T55 labeled populations were severely

impacted by loss of FGF8 likely reflecting abnormal differentiation in combination with the previously reported effects of loss of FGF8 to decrease proliferation and survival in the SHF (Park et al., 2006). It is notable that *Sema3c* was identified in a genome-wide chromatin IP for Islet1 binding sites and is thought to be a regulatory target (Gao et al., 2019). The observed sensitivity of expression of the 96-16 transgene to *Isl1* haploinsufficiency (*Isl1Cre* is a null allele for Islet1) is more severe than its effect on *Sema3c* transcripts seen by *in situ* hybridization; this may reflect the fact that while the insertion site of the transgene is close to *Sema3c*, the transgene is likely only subject to a subset of *Sema3c* regulatory elements. Despite the impact of loss of FGF8 on multiple SHF subdomains, we previously noted that the expression of *Fgf10* was unaffected (Park et al., 2006). Our data indicate that unlike other models where a single outflow vessel from the heart is likely due to pulmonary atresia rather than PTA (Kirby, 2008), the loss of FGF8 signals disrupts the fate of both the subpulmonary and the subaortic myocardial precursors supporting the diagnosis of PTA rather than pulmonary atresia. This is consistent with the finding of 4 and 5 leaflet outflow valves in *Fgf8* and *Fgf receptor* mutants (Frank et al., 2002; Park et al., 2006; Park et al., 2008). Further studies are warranted to determine how FGF8 regulates the fate of additional SHF subdomains during OFT development.

MATERIALS AND METHODS

Mice

The *Isl1Cre* allele (*Isl1*$^{(Cre)Sev}$) was bred into mice bearing the *Fgf8* conditional (*Fgf8*^{tm2Moon}; herein called *Fgf8*^{fl}) and this allele recombined to a null allele (*Fgf8*$^{-}$) to generate *Fgf8* $^{fl/-}$; *Isl1Cre* mutants. *Fgf* $^{fl/+}$ animals served as controls. All mice were maintained in mixed background of SV129 and C57Bl6.

Immunofluorescent detection of antigens in cryosectioned specimens (Figures 1 and 2).

Embryos were fixed in 4%PFA for 2 hours, washed in PBS and then cryoprotected in serial glycerol solutions followed by embedding in OCT. Sections were at 7 microns. Tissue on the slide was then permeabilized with PBST washes, followed by a rinse in PBS. Slides were blocked in 5% donkey serum (d9663 Sigma) in PBST at RT for 30 minutes prior to application of the primary antibody in blocking buffer. Slides were incubated at 4 degrees overnight. Slides were washed in PBST followed by application of secondary antibody in blocking buffer for 2 hours at room temperature and then washed in PBST and mounted with Vectashield prior to imaging. Antibodies used were: Titin - Proteintech 27867-1-AP, 1:200; β-catenin - Thermofisher #712700

1:100; integrin α5 - BD Pharmingen #553319, 1:200; integrin β1 - Millipore, MAB1997, 1:100; Fn1 - Abcam # 199056, 1:500; Podocalyxin - R&D, # AF1556, 1:200; Islet1 - Iowa Developmental Hybridoma Bank, #39.4D5, 1:100; MYH1E (sarcomeric myosin heavy chain) - Iowa Developmental Hybridoma Bank, MF20, 1:100. F-actin was detected with Texas red-conjugated phalloidin (Thermo Fisher Scientific) added to the secondary antibody solution.

Immunofluorescent detection of antigens in paraffin sectioned specimens (Supplemental Figure 1).

Slides were prepared and stained as described in (Francou et al., 2014). Antibodies used were: Scribble (Santa Cruz sc-11049); aPKC-zeta (Santa Cruz sc-216) 1/200.

β-Galactosidase staining

Embryos were fixed in 0.2% glutaraldehyde in PBS, 0.02% NP40 (PBN) on ice for 10 minutes, washed in PBN, and placed in X-gal staining solution (5 mM potassium ferricyanide, 5 mM potassium ferrocyanide, 2 mM $MgCl_2$, 1 mg/ml X-gal, in PBS, pH 7.3). Staining was carried out overnight at room temperature while rocking. After staining, embryos were washed in PBN and post-fixed in 4% paraformaldehyde overnight at 4°C.

Preparation of RNA and cDNA, and performance of microarrays

E9.5 OFTs were dissected and stored in RLT buffer (Qiagen) at −80°C. Seven specimens of each genotype were pooled to generate each sample, as described in (Park et al., 2008). For the SHF, ~180 specimens for each genotype were collected as described in the microdissection/tissue separation protocol below. Total RNA was extracted using RNeasy Micro Kit, Qiagen. Agilent two-color LRILAK labeling, the Agilent two-color GE hybridization/wash protocol, and the Agilent 5-micron XDR scanning protocols were carried out by the University of Utah Microarray Core Facility. For cDNA, RNA (100 ng) was reverse-transcribed to cDNA using the SuperScript III First-Strand Synthesis System (Invitrogen). Quantitative RT-PCR was performed with iQ SYBR Green Supermix on the iCycler system (Bio-Rad).

Microarray analyses

The experiments were run in quadruplicate on Agilent mouse whole-genome expression arrays. The array image data were quantitated using Agilent Feature Extraction software (version 9.5.1.1). Subtle intensity-dependent bias was corrected with LOWESS normalization, with no background subtraction. Statistical analysis of normalized log-transformed data was performed in Gene Sifter (www.genesifter.net). Differentially expressed transcripts were defined (adjusted for multiple testing using the Benjamini and Hochberg method) as $P<0.05$. Spots with an intensity below background were removed prior to statistical analysis. Heat maps were generated using Heatmapper (www.heatmapper.ca).

Separation of germ layers to isolate SHF mesoderm

Modified in the Saijoh lab from Manipulating the mouse embryo 2nd ed.

1) **Solutions—**Tyrode's solution

	(g/l)
NaCl	8.0
KCl	0.2

	(g/l)
NaH2PO4 · 2H2O	0.057
NaHCO3	1.0
Glucose	2.0
CaCl2	0.2
MgCl2 · 6H20	0.1

Pancreatin / Trypsin (PT) solution (g/40ml Tyrode)

Pancreatin (Sigma P3292)	0.5	
Trypsin (Sigma T4799)	0.1	
PVP (MW360, Sigma P5288)	0.2	0.5 %

HEPES buffered DMEM (H-DMEM)

DMEM powder, without phenol red, low glucose. (Sigma, D2902-1Lx10)
Hepes: 10mM, 1.19g / 500ml, 2.38g/ L
10N NaOH for final pH of 7.2.
Filtration recommended. Stored at 4°C.

DNaseI

Deoxyribonuclease I from bovine pancrease, Sigma DN2
Stock: 1mg/ml in 10 mM Tris-HCl, pH 7.5, 50 mM NaCl, 10 mM MgCl2, 1 mM DTT, 50% (v/v) glycerol.
20x CaCl2 stock solution
40mM CaCl2, 1ml
20x MgCl2 stock solution
10 mM MgCl2, 1ml

2) Procedure

- Add 5ul of each CaCl2 and MgCl2 stock solution to 100 µl PT solution
- Two 40 ul drops of 10% FBS in H-DMEM and three 30 µl drops of PT Ca-Mg solution in a 35 ml dish on ice.
- 5% FBS in H-DMEM in 35 cm (bottom) and 2% FBS in H-DMEM 6 cm dish (lid) on ice.
- H-DMEM in 6 cm dish, RT
- 1X PBS in 10 cm dish on ice.

1. The decidua were dissected in cold PBS and place in 5% FBS/H-DMEM soln in 35ml dish on ice.
2. Remove embryos, dissect pharyngeal region in H-DMEM
3. Incubate the tissues in PT Ca-Mg solution on ice for 5 - 6 min. PT solution containing Ca2+, Mg2+ works better for dissociation of the heart because mesoderm cells can keep their structure more tightly and DNase I is activated by Mg2+.
4. Transfer embryos to 15% FBS to stop digestion and incubate for 5 minutes to protect tissue.
5. Separate the germ layers with a tungsten needle and fine forceps in H-DMEM containing 1-2% FBS

Supplementary Material

Refer to Web version on PubMed Central for supplementary material.

ACKNOWLEDGEMENTS

We thank technicians in the Moon lab, Dr. Eon Joo Park, and the University of Utah Program in Molecular Medicine. CA is funded by an AHA postdoctoral fellowship number 836254; SA is funded by NHLBI (R01 HL103920, R01 HL134935, and R01 HL158049).

REFERENCES

Ai D, Fu X, Wang J, Lu MF, Chen L, Baldini A, Klein WH, Martin JF, 2007. Canonical Wnt signaling functions in second heart field to promote right ventricular growth. Proc Natl Acad Sci U S A 104, 9319–9324. [PubMed: 17519332]

Bajolle F, Zaffran S, Kelly RG, Hadchouel J, Bonnet D, Brown NA, Buckingham ME, 2006. Rotation of the myocardial wall of the outflow tract is implicated in the normal positioning of the great arteries. Circ Res 98, 421–428. [PubMed: 16397144]

Bajolle F, Zaffran S, Meilhac SM, Dandonneau M, Chang T, Kelly RG, Buckingham ME, 2008. Myocardium at the base of the aorta and pulmonary trunk is prefigured in the outflow tract of the heart and in subdomains of the second heart field. Dev Biol 313, 25–34. [PubMed: 18005956]

Bartram U, Molin DG, Wisse LJ, Mohamad A, Sanford LP, Doetschman T, Speer CP, Poelmann RE, Gittenberger-de Groot AC, 2001. Double-outlet right ventricle and overriding tricuspid valve reflect disturbances of looping, myocardialization, endocardial cushion differentiation, and apoptosis in TGF-beta(2)-knockout mice. Circulation 103, 2745–2752. [PubMed: 11390347]

Biben C, Hatzistavrou T, Harvey RP, 1998. Expression of NK-2 class homeobox gene Nkx2–6 in foregut endoderm and heart. Mech Dev 73, 125–127. [PubMed: 9545560]

Boyett MR, Inada S, Yoo S, Li J, Liu J, Tellez J, Greener ID, Honjo H, Billeter R, Lei M, Zhang H, Efimov IR, Dobrzynski H, 2006. Connexins in the sinoatrial and atrioventricular nodes. Adv Cardiol 42, 175–197. [PubMed: 16646591]

Buckingham M, Meilhac S, Zaffran S, 2005. Building the mammalian heart from two sources of myocardial cells. Nat Rev Genet 6, 826–835. [PubMed: 16304598]

Cai CL, Martin JC, Sun Y, Cui L, Wang L, Ouyang K, Yang L, Bu L, Liang X, Zhang X, Stallcup WB, Denton CP, McCulloch A, Chen J, Evans SM, 2008. A myocardial lineage derives from Tbx18 epicardial cells. Nature 454, 104–108. [PubMed: 18480752]

Chen YH, Ishii M, Sun J, Sucov HM, Maxson RE Jr., 2007. Msx1 and Msx2 regulate survival of secondary heart field precursors and post-migratory proliferation of cardiac neural crest in the outflow tract. Dev Biol 308, 421–437. [PubMed: 17601530]

Christoffels VM, Habets PE, Franco D, Campione M, de Jong F, Lamers WH, Bao ZZ, Palmer S, Biben C, Harvey RP, Moorman AF, 2000. Chamber formation and morphogenesis in the developing mammalian heart. Dev Biol 223, 266–278. [PubMed: 10882515]

Cohen ED, Wang Z, Lepore JJ, Lu MM, Taketo MM, Epstein DJ, Morrisey EE, 2007. Wnt/beta-catenin signaling promotes expansion of Isl-1-positive cardiac progenitor cells through regulation of FGF signaling. J Clin Invest 117, 1794–1804. [PubMed: 17607356]

de la Cruz MV, Markwald RR, Krug EL, Rumenoff L, Sanchez Gomez C, Sadowinski S, Galicia TD, Gomez F, Salazar Garcia M, Villavicencio Guzman L, Reyes Angeles L, Moreno-Rodriguez RA, 2001. Living morphogenesis of the ventricles and congenital pathology of their component parts. Cardiol Young 11, 588–600. [PubMed: 11813909]

de la Cruz MV, Sanchez Gomez C, Arteaga MM, Arguello C, 1977. Experimental study of the development of the truncus and the conus in the chick embryo. J Anat 123, 661–686. [PubMed: 885781]

Francou A, Saint-Michel E, Mesbah K, Kelly RG, 2014. TBX1 regulates epithelial polarity and dynamic basal filopodia in the second heart field. Development 141, 4320–4331. [PubMed: 25371366]

Frank DU, Carter KL, Thomas KR, Burr RM, Bakker ML, Coetzee WA, Tristani-Firouzi M, Bamshad MJ, Christoffels VM, Moon AM, 2012. Lethal arrhythmias in Tbx3-deficient mice reveal extreme dosage sensitivity of cardiac conduction system function and homeostasis. Proc Natl Acad Sci U S A 109, E154–163. [PubMed: 22203979]

Frank DU, Fotheringham LK, Brewer JA, Muglia LJ, Tristani-Firouzi M, Capecchi MR, Moon AM, 2002. An Fgf8 mouse mutant phenocopies human 22q11 deletion syndrome. Development 129, 4591–4603. [PubMed: 12223415]

Gao R, Liang X, Cheedipudi S, Cordero J, Jiang X, Zhang Q, Caputo L, Gunther S, Kuenne C, Ren Y, Bhattacharya S, Yuan X, Barreto G, Chen Y, Braun T, Evans SM, Sun Y, Dobreva G, 2019. Pioneering function of Isl1 in the epigenetic control of cardiomyocyte cell fate. Cell Res 29, 486–501. [PubMed: 31024170]

Guo C, Sun Y, Zhou B, Adam RM, Li X, Pu WT, Morrow BE, Moon A, 2011. A Tbx1-Six1/Eya1-Fgf8 genetic pathway controls mammalian cardiovascular and craniofacial morphogenesis. J Clin Invest 121, 1585–1595. [PubMed: 21364285]

Hamblet NS, Lijam N, Ruiz-Lozano P, Wang J, Yang Y, Luo Z, Mei L, Chien KR, Sussman DJ, Wynshaw-Boris A, 2002. Dishevelled 2 is essential for cardiac outflow tract development, somite segmentation and neural tube closure. Development 129, 5827–5838. [PubMed: 12421720]

Heathcote K, Braybrook C, Abushaban L, Guy M, Khetyar ME, Patton MA, Carter ND, Scambler PJ, Syrris P, 2005. Common arterial trunk associated with a homeodomain mutation of NKX2.6. Hum Mol Genet 14, 585–593. [PubMed: 15649947]

Kelly RG, Brown NA, Buckingham ME, 2001. The arterial pole of the mouse heart forms from Fgf10-expressing cells in pharyngeal mesoderm. Dev Cell 1, 435–440. [PubMed: 11702954]

Kibar Z, Vogan KJ, Groulx N, Justice MJ, Underhill DA, Gros P, 2001. Ltap, a mammalian homolog of Drosophila Strabismus/Van Gogh, is altered in the mouse neural tube mutant Loop-tail. Nat Genet 28, 251–255. [PubMed: 11431695]

Kim KH, Rosen A, Bruneau BG, Hui CC, Backx PH, 2012. Iroquois homeodomain transcription factors in heart development and function. Circ Res 110, 1513–1524. [PubMed: 22628575]

Kioussi C, Briata P, Baek SH, Rose DW, Hamblet NS, Herman T, Ohgi KA, Lin C, Gleiberman A, Wang J, Brault V, Ruiz-Lozano P, Nguyen HD, Kemler R, Glass CK, Wynshaw-Boris A, Rosenfeld MG, 2002. Identification of a Wnt/Dvl/beta-Catenin --> Pitx2 pathway mediating cell-type-specific proliferation during development. Cell 111, 673–685. [PubMed: 12464179]

Kirby ML, 2008. Pulmonary atresia or persistent truncus arteriosus: is it important to make the distinction and how do we do it? Circ Res 103, 337–339. [PubMed: 18703785]

Li D, Angermeier A, Wang J, 2019. Planar cell polarity signaling regulates polarized second heart field morphogenesis to promote both arterial and venous pole septation. Development 146.

Liao J, Aggarwal VS, Nowotschin S, Bondarev A, Lipner S, Morrow BE, 2008. Identification of downstream genetic pathways of Tbx1 in the second heart field. Dev Biol 316, 524–537. [PubMed: 18328475]

Lin L, Cui L, Zhou W, Dufort D, Zhang X, Cai CL, Bu L, Yang L, Martin J, Kemler R, Rosenfeld MG, Chen J, Evans SM, 2007. Beta-catenin directly regulates Islet1 expression in cardiovascular progenitors and is required for multiple aspects of cardiogenesis. Proc Natl Acad Sci U S A 104, 9313–9318. [PubMed: 17519333]

Lough J, Sugi Y, 2000. Endoderm and heart development. Dev Dyn 217, 327–342. [PubMed: 10767078]

Meder D, Shevchenko A, Simons K, Fullekrug J, 2005. Gp135/podocalyxin and NHERF-2 participate in the formation of a preapical domain during polarization of MDCK cells. J Cell Biol 168, 303–313. [PubMed: 15642748]

Meilhac SM, Esner M, Kelly RG, Nicolas JF, Buckingham ME, 2004. The clonal origin of myocardial cells in different regions of the embryonic mouse heart. Dev Cell 6, 685–698. [PubMed: 15130493]

Mittal A, Pulina M, Hou SY, Astrof S, 2010. Fibronectin and integrin alpha 5 play essential roles in the development of the cardiac neural crest. Mech Dev 127, 472–484. [PubMed: 20807571]

Mittal A, Pulina M, Hou SY, Astrof S, 2013. Fibronectin and integrin alpha 5 play requisite roles in cardiac morphogenesis. Dev Biol 381, 73–82. [PubMed: 23791818]

Mjaatvedt CH, Nakaoka T, Moreno-Rodriguez R, Norris RA, Kern MJ, Eisenberg CA, Turner D, Markwald RR, 2001. The outflow tract of the heart is recruited from a novel heart-forming field. Dev Biol 238, 97–109. [PubMed: 11783996]

Montcouquiol M, Rachel RA, Lanford PJ, Copeland NG, Jenkins NA, Kelley MW, 2003. Identification of Vangl2 and Scrb1 as planar polarity genes in mammals. Nature 423, 173–177. [PubMed: 12724779]

Ojakian GK, Schwimmer R, 1988. The polarized distribution of an apical cell surface glycoprotein is maintained by interactions with the cytoskeleton of Madin-Darby canine kidney cells. J Cell Biol 107, 2377–2387. [PubMed: 3198692]

Park EJ, Ogden LA, Talbot A, Evans S, Cai CL, Black BL, Frank DU, Moon AM, 2006. Required, tissue-specific roles for Fgf8 in outflow tract formation and remodeling. Development 133, 2419–2433. [PubMed: 16720879]

Park EJ, Watanabe Y, Smyth G, Miyagawa-Tomita S, Meyers E, Klingensmith J, Camenisch T, Buckingham M, Moon AM, 2008. An FGF autocrine loop initiated in second heart field mesoderm regulates morphogenesis at the arterial pole of the heart. Development 135, 3599–3610. [PubMed: 18832392]

Phillips HM, Rhee HJ, Murdoch JN, Hildreth V, Peat JD, Anderson RH, Copp AJ, Chaudhry B, Henderson DJ, 2007. Disruption of planar cell polarity signaling results in congenital heart defects and cardiomyopathy attributable to early cardiomyocyte disorganization. Circ Res 101, 137–145. [PubMed: 17556662]

Rochais F, Dandonneau M, Mesbah K, Jarry T, Mattei MG, Kelly RG, 2009. Hes1 is expressed in the second heart field and is required for outflow tract development. PLoS One 4, e6267. [PubMed: 19609448]

Ruiz-Villalba A, Hoppler S, van den Hoff MJ, 2016. Wnt signaling in the heart fields: Variations on a common theme. Dev Dyn 245, 294–306. [PubMed: 26638115]

Sandireddy R, Cibi DM, Gupta P, Singh A, Tee N, Uemura A, Epstein JA, Singh MK, 2019. Semaphorin 3E/PlexinD1 signaling is required for cardiac ventricular compaction. JCI Insight 4.

Schultheiss TM, Xydas S, Lassar AB, 1995. Induction of avian cardiac myogenesis by anterior endoderm. Development 121, 4203–4214. [PubMed: 8575320]

Shou W, Aghdasi B, Armstrong DL, Guo Q, Bao S, Charng MJ, Mathews LM, Schneider MD, Hamilton SL, Matzuk MM, 1998. Cardiac defects and altered ryanodine receptor function in mice lacking FKBP12. Nature 391, 489–492. [PubMed: 9461216]

Sinha T, Wang B, Evans S, Wynshaw-Boris A, Wang J, 2012. Disheveled mediated planar cell polarity signaling is required in the second heart field lineage for outflow tract morphogenesis. Dev Biol 370, 135–144. [PubMed: 22841628]

Theveniau-Ruissy M, Dandonneau M, Mesbah K, Ghez O, Mattei MG, Miquerol L, Kelly RG, 2008. The del22q11.2 candidate gene Tbx1 controls regional outflow tract identity and coronary artery patterning. Circ Res 103, 142–148. [PubMed: 18583714]

Urness LD, Bleyl SB, Wright TJ, Moon AM, Mansour SL, 2011. Redundant and dosage sensitive requirements for Fgf3 and Fgf10 in cardiovascular development. Dev Biol 356, 383–397. [PubMed: 21664901]

Vincentz JW, McWhirter JR, Murre C, Baldini A, Furuta Y, 2005. Fgf15 is required for proper morphogenesis of the mouse cardiac outflow tract. Genesis 41, 192–201. [PubMed: 15789410]

Waldo KL, Kumiski DH, Wallis KT, Stadt HA, Hutson MR, Platt DH, Kirby ML, 2001. Contoruncal myocardium arises from a secondary heart field. Development 128, 3179–3188. [PubMed: 11688566]

Watanabe Y, Zaffran S, Kuroiwa A, Higuchi H, Ogura T, Harvey RP, Kelly RG, Buckingham M, 2012. Fibroblast growth factor 10 gene regulation in the second heart field by Tbx1, Nkx2–5, and Islet1 reveals a genetic switch for down-regulation in the myocardium. Proc Natl Acad Sci U S A 109, 18273–18280. [PubMed: 23093675]

Yamamoto S, Nishimura O, Misaki K, Nishita M, Minami Y, Yonemura S, Tarui H, Sasaki H, 2008. Cthrc1 selectively activates the planar cell polarity pathway of Wnt signaling by stabilizing the Wnt-receptor complex. Dev Cell 15, 23–36. [PubMed: 18606138]

Yutzey KE, Kirby ML, 2002. Wherefore heart thou? Embryonic origins of cardiogenic mesoderm. Dev. Dynamics 223, 307–320.

Zaffran S, Kelly RG, Meilhac SM, Buckingham ME, Brown NA, 2004. Right ventricular myocardium derives from the anterior heart field. Circ Res 95, 261–268. [PubMed: 15217909]

Zhou B, Ma Q, Rajagopal S, Wu SM, Domian I, Rivera-Feliciano J, Jiang D, von Gise A, Ikeda S, Chien KR, Pu WT, 2008. Epicardial progenitors contribute to the cardiomyocyte lineage in the developing heart. Nature.

Zhou W, Lin L, Majumdar A, Li X, Zhang X, Liu W, Etheridge L, Shi Y, Martin J, Van de Ven W, Kaartinen V, Wynshaw-Boris A, McMahon AP, Rosenfeld MG, Evans SM, 2007. Modulation of morphogenesis by noncanonical Wnt signaling requires ATF/CREB family-mediated transcriptional activation of TGFbeta2. Nat Genet 39, 1225–1234. [PubMed: 17767158]

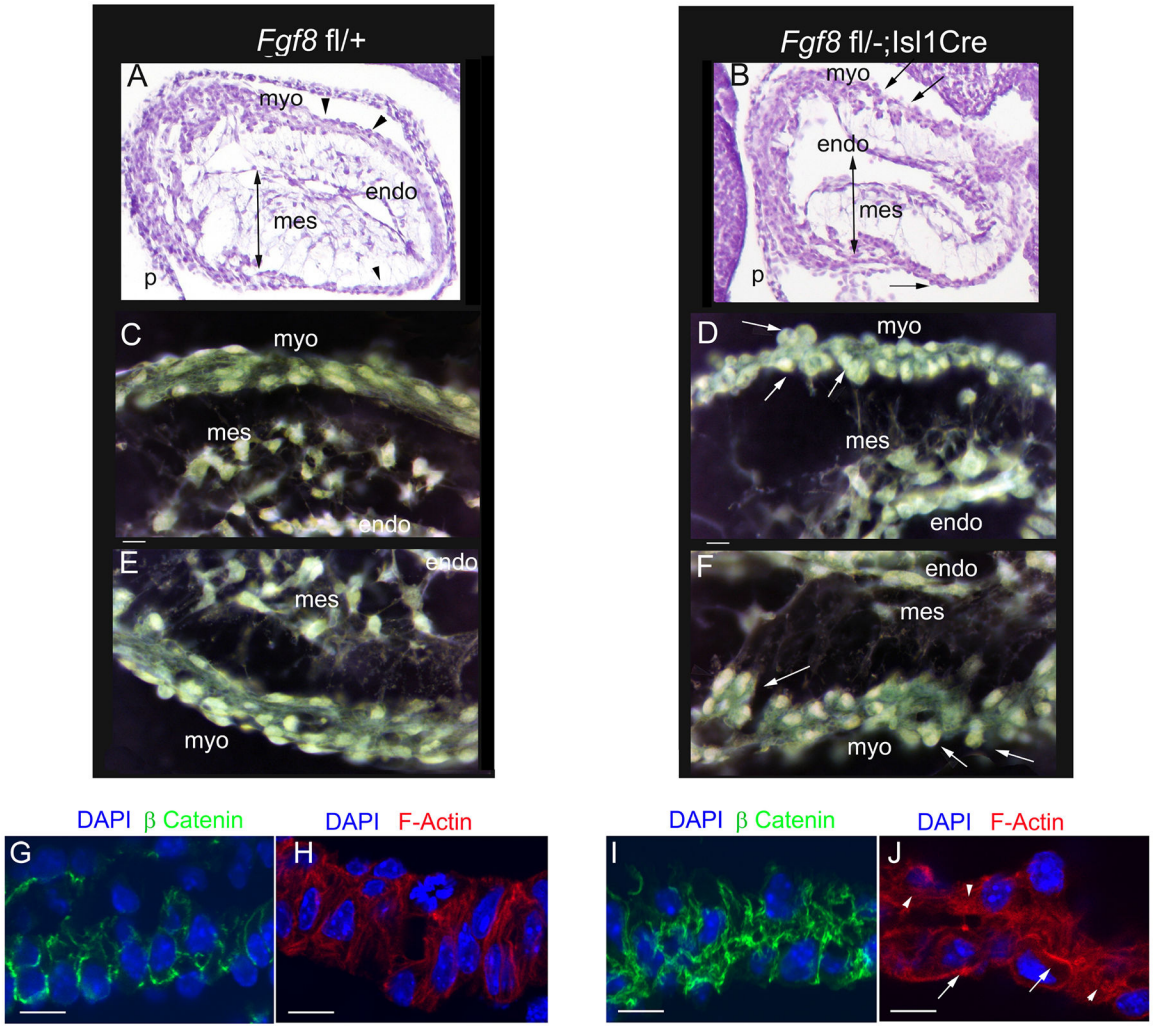

Figure 1. Loss of FGF8 results in abnormal cellular organization of the embryonic outflow tract myocardium.

A, B) Bright field 20X images of H&E-stained transverse sections through the outflow tract of e10.5 control and *Fgf8* mutant embryos; genotypes are indicated at top. Orientation is right at top, left at bottom; proximal OFT on left, distal OFT on right. Hearts were relaxed with verapamil at time of harvest. Double ended black arrow is 150 microns in both A and B and highlights paucity of cushion jelly and mesenchymal cells in the mutant. Arrowheads in A highlight smooth epithelial organization of myocardium while arrows in B highlight disorganized myocardium with out-of-plane cells.

C-F) Dark field images of the OFT walls of additional embryos showing rounded, out of plane myocardial cells in mutants and reproducibility of findings shown in A and B. C and D are right OFT walls, E and F are left walls. Scale bars are 10 microns.

G-J) Confocal images of sagittal sections through the myocardium of the distal OFT stained for DNA (DAPI, blue), β-catenin (green, G, I) and filamentous actin (H, J). Scale bars are 10 microns. Note aligned, parallel actin stained fibers in H, while arrows in J denote pericellular actin staining and arrowheads highlight disorganized cytoplasmic staining in the mutant OFT.

myo, myocardium; endo, outflow tract endothelium; mes, outflow tract mesenchyme in the endocardial cushions consisting of cardiac jelly and EMT-derived mesenchymal cells; p, pericardium.

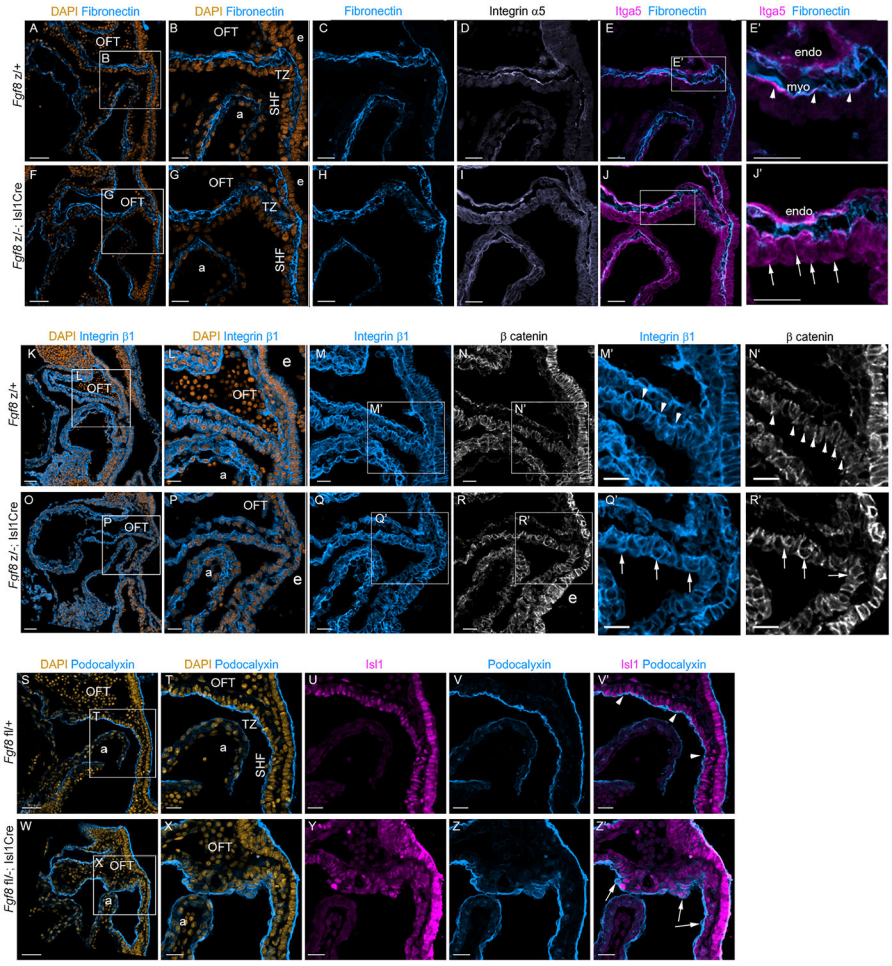

Figure 2. Loss of FGF8 disrupts basement membrane deposition, cell polarity and cellular organization in the SHF and OFT.

A-J') Confocal images of sagittal sections through the OFT, transition zone/SHF of control (A-E') and *Fgf8* mutant (F-J') E9.5 embryos. DNA is stained with DAPI (orange). Immunohistochemistry was used to detect fibronectin (blue), and Integrin α5 (pink). Arrowheads in E' highlight fibronectin and Itgα5 normally assembled and adjacent in the OFT basement membrane (basal surface); arrows in J' in the mutant highlight Itgα5 aberrantly localized throughout the cell membrane, independent of fibronectin, which is decreased.

Scale bars are 50 μM in A and F and 20 μM in all other panels. B-E and F-J are digital zoom images of the boxed areas in A and H. E' and J' are digital zoom images of the boxed areas in E and J. Images are representative of ≥ 3 embryos.

OFT, distal outflow tract lumen; a, right atrium; TZ, transition zone; SHF, second heart field; endo, endoderm; myo, myocardium

K-R') Confocal images of sagittal sections through the OFT and SHF of control (K-N') and *Fgf8* mutant (O-R') E9.5 embryos. Immunohistochemistry was used to detect Itgβ1 (blue) and β-catenin (grayscale). DNA is stained with DAPI (orange). Arrowheads in M' and N' indicate normal localization of Itgβ1 in basement membrane (basal surface) of control OFT myocardium and of β-catenin predominantly localized in discrete adhesions, respectively.

Arrows in Q' and R' highlight aberrantly localized Itgβ1 and β-catenin surrounding and at the apical surfaces of cells of the OFT and TZ. The intensity of β-catenin staining is increased in these regions relative to control. Scale bars are 50 μM in K and O and 20 μM in all other panels. K and O are 20X magnifications; all others are digital zoom images as indicated. Results are representative of ≥ 3 embryos.

S-Z') Confocal images of sagittal sections through the OFT and SHF of control (S-V') and *Fgf8* mutant (W-Z') E9.5 embryos. Immunohistochemistry was used to detect the apical marker podocalyxin (blue) and Isl1 (pink). DNA is stained with DAPI (orange). Arrowheads in V' highlight sharp apical localization of podocalyxin along the myocardium of the OFT, TZ and SHF. Arrows in J indicate abnormal clusters of disorganized mesoderm cells with pericellular podocalyxin staining. S and W are 20X magnifications; all others are digital zoom images of the boxed areas in S and W.

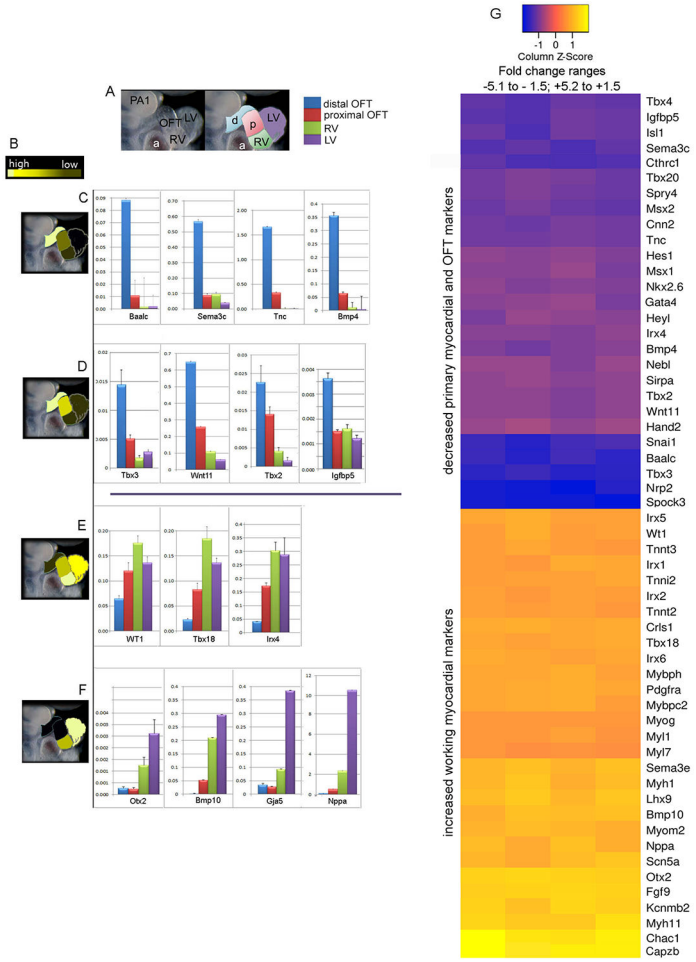

Figure 3. The outflow tract myocardium in *Fgf8* mutants has an abnormal working myocardial transcriptional profile.

A) Right lateral view of E9.5 embryo hearts with segments of heart labeled and color key PA1, pharyngeal arch 1 a, right atrium; OFT, outflow tract (d, distal p, proximal); RV right ventricle; LV left ventricle

B-F) Schematics of patterns of transcript levels in different heart segments colored from high (pale yellow) to low (black). Schematics are shown adjacent to graphs quantitating transcript levels from representative transcripts in that class.

C) qRT-PCR control reveals a pattern of high expression in the distal OFT relative to all other segments for transcript levels of *Baalc, Sema3c, Tnc,* and *Bmp4* relative to *HPRT*.

D) qRT-PCR reveals a pattern in this group highest in distal OFT, graded to proximal OFT with increased levels in the proximal OFT and ventricles compared to group C for *Tbx3, Wnt11, Tbx2 and Igfbp5* transcripts.

E) qRT-PCR results of transcript levels of *WT1, Tbx18, Irx4* show pattern in which distal OFT has low expression levels, proximal OFT next and levels in the RV and LV are higher and comparable to one another.

F) qRT-PCR results of transcript levels of *Otx2, Bmp10, Gja5* and *Nppa* relative to HPRT control. The pattern in this group is highest in LV, lower in RV and minimally expressed in either segment of the OFT.

G) Heat map of fold change values for significantly dysregulated OFT and chamber/working myocardial genes in microdissected OFTs of *Fgf8* mutants relative to controls. The range of values was −5.1 to −1.5 for downregulated genes and +1.5 to +5.1 for the upregulated genes. Note levels for working myocardial genes are increased (yellow shades) in the mutant OFT while OFT/nonworking markers are decreased.

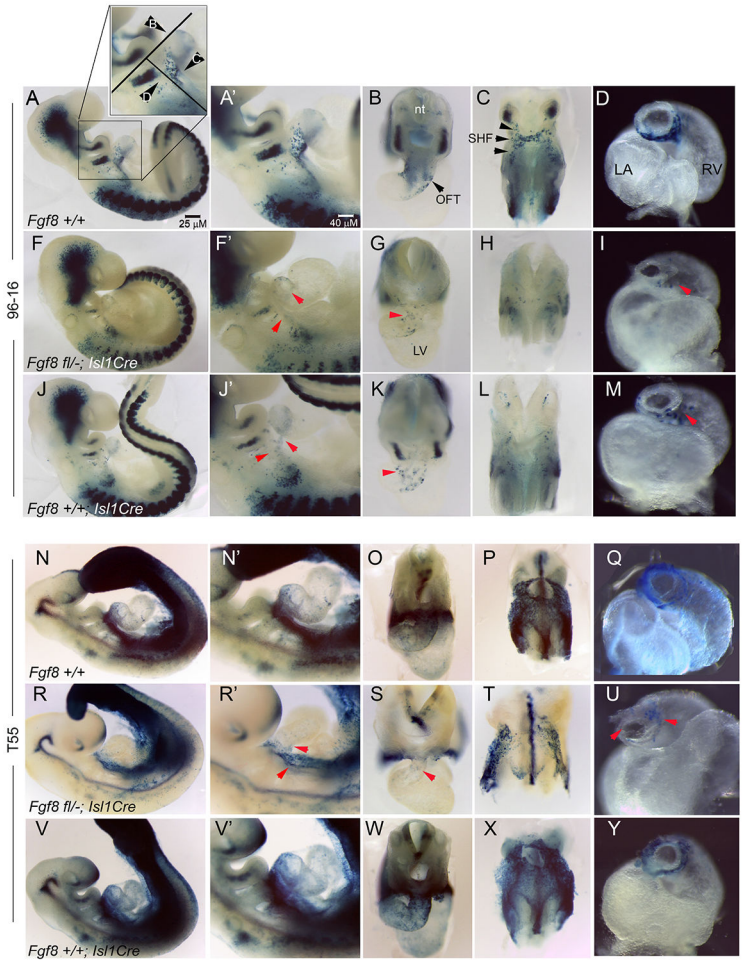

Figure 4. Expression of the 96-16 and T55 SHF subregion transgenic reporters is altered in *Fgf8* mutants.

Images show whole mount and dissected E9.5 embryos after staining for β-galactosidase activity driven by the 96-16 (A-M) and T55 (N-Y) transgenes. Genotypes are indicated at lower left of first panel in each row.

A/ A', F/F', J/J', N/N', R/R' and V/V' are right lateral views; scale bars for these images are shown in lower right of panel A and A'. Red arrowheads in F', J' and R' highlight decreased lacZ staining in OFT and SHF.

B, G, K, O, S and W show caudal portion of body after transverse dissection through the second pharyngeal arch as in the diagram to the top of panel A. The view of these panels is from the vantage indicated by black arrowhead labeled B in the diagram. The neural tube (nt) is at top of the image; embryo's right is on the left. Red arrowheads in G, K and S highlight decreased staining in OFT.

C, H, L, P, T, and X are images of the embryo body after removal of the heart in plane indicated in diagram viewed in direction indicated by black arrowhead labeled C in diagram.

D, I, M, Q, U and Y are images of dissected heart/OFT from the vantage indicated by arrowhead labeled D in diagram. The ventral aspect of the heart is at top. LA, left atrium; RA, right atrium

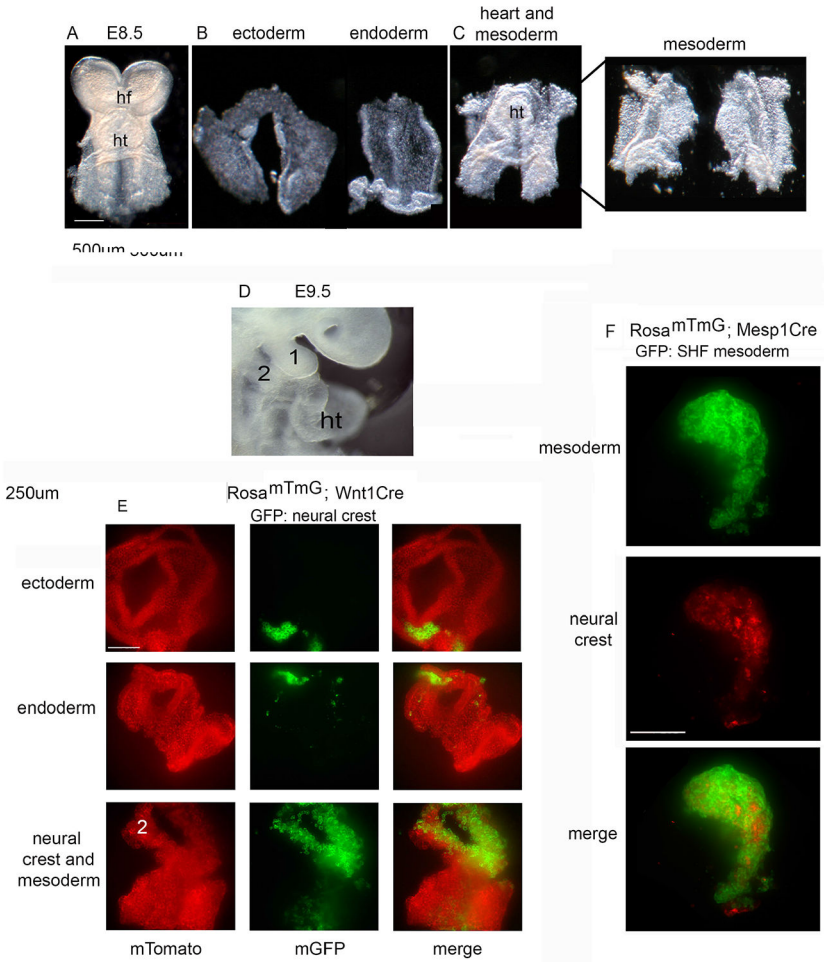

Figure 5. Microdissection and separation of pharyngeal tissue layers, including SHF.

A-C) Illustration of microdissection performed on an E8.5 embryo. Scale bar 500 μM.

D) Right sided view of whole mount E9.5 wild type embryo. HT, Heart; pharyngeal arches 1 and 2 are labeled; ht, heart.

E) Microdissection of tissue layers in *Wnt1Cre; Rosa* ^{mTmG} E9.5 embryos to label neural crest green. Scale bar 250 μM.

F) Microdissection of SHF/second pharyngeal arch in *Mesp1Cre; Rosa* ^{mTmG} E9.5 embryos to label mesoderm green. Note residual neural crest in dissected region in red. Scale bar 250 μM. 2, pharyngeal arch 2

Figure 6. Outflow tract progenitors in the second heart field aberrantly express working myocardial transcripts and proteins in the absence of FGF8.

A) Heatmap of log2 fold change values of significantly dysregulated myocardial and progenitor genes in SHF microdissected from *Fgf8* mutants compared to controls. The range of Log2 values is +0.51 to +4.3 (1.5 to 19.6 fold) for the upregulated genes and −2.3 to −0.51 and (−4.9 to −1.5 fold) for the downregulated genes. Black arrowheads at left denote transcripts that were similarly dysregulated in mutant OFT.

B-G) Immunofluorescence detection of Titin and MF-20 in sagittal sections through the outflow tract and second heart field of E9.5 controls (B, D, F) and *Fgf8* mutants (C, E, G) and Titin is in blue, MF-20 in pink and DAPI in orange. D-F show high magnification views of the TZ/SHF. Arrows point out minimal-to-no signal for either marker in the TZ/SHF of the control and presence of signal in this region in the mutants.

RA, right atrium; OFT, outflow tract; RV, right ventricle; TZ/SHF, transition zone/second heart field